Petroleum Science 21 (2024) 2407–2419

Contents lists available at ScienceDirect

Petroleum Science

journal homepage: www.keaipublishing.com/en/journals/petroleum-science

Original Paper

Influence of pore structure heterogeneity on channeling channels during hot water flooding in heavy oil reservoir based on CT scanning

Qing-Jun Du [a, b], Hao-Yu Zheng [a, b], Jian Hou [a, b, c, *], Yong-Ge Liu [a, b], Jian-Fang Sun [d], Dong Zhao [a, b]

[a] State Key Laboratory of Deep Oil and Gas, China University of Petroleum (East China), Qingdao, 266580, Shandong, PR China
[b] School of Petroleum Engineering, China University of Petroleum (East China), Qingdao, 266580, Shandong, PR China
[c] Laboratory for Marine Mineral Resources, Qingdao National Laboratory for Marine Science and Technology, Qingdao, 266237, Shandong, PR China
[d] Petroleum Exploration and Production Research Institute, SINOPEC, Beijing, 10083, PR China

ARTICLE INFO

Article history:
Received 5 November 2023
Received in revised form
18 February 2024
Accepted 19 March 2024
Available online 22 March 2024

Edited by Meng-Jiao Zhou

Keywords:
Heavy oil
Hot water flooding
Pore structure
Channeling channels
CT scanning

ABSTRACT

Hot water flooding is an effective way to develop heavy oil reservoirs. However, local channeling channels may form, possibly leading to a low thermal utilization efficiency and high water cut in the reservoir. The pore structure heterogeneity is an important factor in forming these channels. This study proposes a method that mixes quartz sand with different particle sizes to prepare weakly heterogeneous and strongly heterogeneous models through which hot water flooding experiments are conducted. During the experiments, computer tomography (CT) scanning identifies the pore structure and micro remaining oil saturation distribution to analyze the influence of the pore structure heterogeneity on the channeling channels. The oil saturation reduction and average pore size are divided into three levels to quantitatively describe the relationship between the channeling channel distribution and pore structure heterogeneity. The zone where oil saturation reduction exceeds 20% is defined as a channeling channel. The scanning area is divided into 180 equally sized zones based on the CT scanning images, and three-dimensional (3D) distributions of the channeling channels are developed. Four micro remaining oil distribution patterns are proposed, and the morphology characteristics of micro remaining oil inside and outside the channeling channels are analyzed. The results show that hot water flooding is more balanced in the weakly heterogeneous model, and the oil saturation decreases by more than 20% in most zones without narrow channeling channels forming. In the strongly heterogeneous model, hot water flooding is unbalanced, and three narrow channeling channels of different lengths form. In the weakly heterogeneous model, the oil saturation reduction is greater in zones with larger pores. The distribution range of the average pore size is larger in the strongly heterogeneous model. The network remaining oil inside the channeling channels is less than outside the channeling channels, and the hot water converts the network remaining oil into cluster, film, and droplet remaining oil.

1. Introduction

Heavy oil development has become a key issue with increasing energy demands (Liu and Dong, 2022; Sun et al., 2020). The extraction methods of heavy oil include cold and thermal recoveries (Xu et al., 2020; Chen et al., 2023; Wang et al., 2020; Li et al., 2023). Cold recovery has strict requirements for the viscosity range of heavy oil. Thus, the thermal recovery effect is better at high heavy oil viscosities. Thermal oil recovery includes steam huff-n-puff, steam flooding, steam assisted gravity drainage (SAGD), and others (Dong et al., 2019, 2022; Wang et al., 2021; Liu et al., 2023).

Compared with these commonly used displacement methods, hot water flooding has the advantages of low cost, low mobility, and simple processes. Hot water flooding is an economic and reasonable development method for conventional heavy oil reservoirs with low viscosities (Masoomi and Torabi, 2022; Zhang et al., 2022). However, hot water channeling channels form easily because of the

* Corresponding author. State Key Laboratory of Deep Oil and Gas, China University of Petroleum (East China), Qingdao, 266580, Shandong, PR China.
E-mail address: houjian@upc.edu.cn (J. Hou).

https://doi.org/10.1016/j.petsci.2024.03.014

high water-oil mobility ratio and high permeability zones (Zhao and Gates, 2015). In addition, the severe heterogeneity in the pore structure accelerates the fingering of hot water and reduces the breakthrough time. The water cut rapidly increases after forming the channeling channels, and the development performance is poor (Lin et al., 2023; Leng et al., 2022).

Heterogeneity is a major challenge when developing oil and gas reservoirs (Li et al., 2018a; Hu et al., 2023; Ado et al., 2019). Microscale heterogeneity is caused primarily by deposition conditions and the secondary effects of reservoirs. In China, heavy oil reservoirs with severe heterogeneity are predominantly composed of terrestrial clastic sediments, with significant differences in the pore throat sizes at various locations. Much recent scientific research has been conducted on the micro-scale heterogeneity of reservoirs, focusing on both physical experiments and numerical simulations (Rezaeiakmal et al., 2022; Liu et al., 2018; Ding et al., 2022a). Oil displacement experiments in rock cores are the most common method for studying the heterogeneity of pore structures. Li et al. (2022) conducted CO_2 gas channeling experiments on parallel short cores (matrix) with different permeability ratios and parallel long cores of various fracture conductivities to study the supercritical CO_2 miscible flooding performance in heterogeneous reservoirs. Ding et al. (2022b) conducted core flooding experiments in heterogeneous carbonate rock and explored the feasibility of foam-enhanced oil recovery. Li et al. (2018b) performed oil displacement experiments in rock cores and established a pore network model to characterize the microheterogeneity of pore structures and the remaining oil distribution after displacement. The work expanded on the relationship between the remaining oil distribution and the pore structure heterogeneity. Sun et al. (2021) conducted CT scanning on core samples of different categories to analyze the impact of pore heterogeneity on the micro remaining oil distribution in clastic reservoirs. Wei et al. (2018) performed gas-flooding and foam-flooding experiments in severely heterogeneous cores to study the enhanced oil recovery performance of gas and foam in heterogeneous reservoirs.

Visualization experiments are a common research method employing micro models for core flooding experiments. Wang et al. (2022) established a visual micromodel with three permeability zones to conduct experiments and analyze the multiphase flow characteristics and mechanisms for enhancing oil recovery in reservoirs with microscale heterogeneity. Zhao et al. (2022) used glass etching models to simulate fractured and porous reservoirs. The influence of heterogeneity on the migration patterns of water flooding was studied by analyzing the water flooding front morphology. Numerical simulations also play a significant role in studying pore structure heterogeneity. Wang et al. (2023) proposed a method for quantitatively characterizing and adjusting the flow field in heterogeneous reservoirs in the late stage of water flooding. Thus, they investigated the influence of heterogeneity on the flow field distribution and remaining oil. Spooner et al. (2021) derived new metrics (the dynamic Lorenz coefficient L) to assess the dynamic heterogeneity in fractured reservoirs. The influence of the pore structure heterogeneity on the remaining oil distribution is one of the hot topics. However, current research mainly uses cores of differing permeabilities for experiments to compare the final oil displacement efficiency and remaining oil distribution. Research on the influence of the internal pore structure heterogeneity of reservoirs on channeling channels and the remaining oil distribution is necessary.

The distribution of micro remaining oil is closely related to the heterogeneity of the pore structure. It is necessary to accurately characterize the associated morphological characteristics and distribution patterns to study the influence of the pore structure heterogeneity on the micro remaining oil distribution. CT scanning is a standard method for studying the distribution pattern of micro remaining oil and has been applied in water flooding, gas flooding, polymer flooding, etc. Cheng et al. (2021) conducted oil displacement experiments and obtained 3D images of the samples using CT scanning. The occurrence characteristics of the remaining oil under different flow rates were studied through image processing and classification. Guo et al. (2018) conducted water flooding experiments on four sandstone samples with different permeabilities, quantified the complexity of pore structures using fractal dimensions, and divided the micro remaining oil into five types using the shape factor and Euler number.

The influence of the pore structure and permeability scale on oil recovery and remaining oil cluster morphology has also been studied. Liu et al. (2021) conducted oil displacement experiments using water flooding, CH_4 flooding, and CO_2 flooding to obtain three remaining oil distribution patterns through CT scanning and image processing. The volume proportions of the three remaining oil types under the three displacement methods were analyzed. Fang et al. (2022) conducted polymer flooding experiments using photolithography glass models and micro-CT scanning techniques with polymers of different molecular weights. Hou et al. (2009) used CT to study the microflow mechanism of polymer flooding and realized 3D visualization of oil-water distributions under various oil displacement conditions through image processing. Yang et al. (2020) injected polymer after 10 pore volume (PV) of water flooding and used CT to obtain the remaining oil distribution at different times. Differences in the remaining oil distribution after water and polymer flooding were compared.

CT scanning is also widely used to study remaining oil in reservoirs for different rock types. Yang et al. (2023) selected sandstone reservoir samples to construct a pore network model using digital rock cores. The influence of pore structure on discontinuous oil phase flow patterns was studied based on 3D CT scanning. Jing et al. (2022) conducted water flooding experiments using three heterogeneous marine carbonate rock samples. They used CT scanning on oil-saturated samples and samples injected with 3, 5, 10, and 20 PV formation water to reconstruct 3D images. The types of remaining oil were classified using shape factors and Euler numbers. Gu et al. (2019) prepared core samples in ultra-low permeability formations with images of the remaining oil using CT scanning technology. Then, the shape and relative volume factors quantified the micro-occurrence state of the remaining oil. Jiang et al. (2022) studied the remaining oil distribution after fracturing flooding using nuclear magnetic resonance (NMR), laser confocal scanning, and CT scanning techniques. Thus, CT scanning has become one of the common methods when studying the remaining oil distribution patterns. However, the experimental environments have limited the application of CT scanning in heavy oil thermal recovery. The temperature and pressure conditions bring further difficulties to CT scanning.

This study proposes a strongly heterogeneous model filled with quartz sand with different particle sizes to replace multiple models of differing permeabilities and simulate the heterogeneous pore structure of reservoirs. Hot water flooding experiments provide the pore structure from the models and remaining oil distribution combined with CT scanning. Zonal statistics on the 3D image obtained from CT scanning divide the results into 180 zones with calculations for the average pore size, remaining oil saturation, and oil saturation reduction in each zone. Differences in the average pore size between the various zones help characterize the heterogeneity of the pore structure. The position and morphology of the channeling channels are characterized based on the oil saturation reduction in the zones. Comparing the average pore size and remaining oil saturation within each zone allows for determining the influence of the pore structure heterogeneity on the remaining

oil distribution and channeling channel morphology. This study provides a theoretical basis for blocking and controlling channeling channels. The poor stability of the sand pack models gives slight changes in the position of quartz sand during displacement. Therefore, CT scanning images at the last moment of flooding are used in each experiment.

2. Experiments

2.1. Apparatus

The experimental setup shown in Fig. 1 consists of a displacement pump, intermediate container, oven, valves, sand pack, temperature sensors, and pressure sensors. The valve inlets are connected to the intermediate container with water and oil. The valve outlets are connected to the sand pack, which is connected to a graduated cylinder for collecting the fluids. The intermediate container and sand pack are placed inside the oven to maintain the experimental temperature. Temperature sensors are connected to the sand pack inlet to ensure the desired temperature of the injected hot water. Pressure sensors measure pressure differences at the sand pack inlet and outlet. A CT scanner (Zeiss Xradia 515 Versa, Germany) and a workstation are required as auxiliary setup. The CT scanner collects images for the samples, and the workstation processes the images.

The sand pack consists of a temperature-resistant, low-density material that can withstand a maximum temperature of 180 °C under normal pressure. During CT scanning, X-rays emitted by the radiation source pass through the material and are received by the detector, producing clear scanning slices. The cavity diameter of the sand pack is 0.6 cm, with a length of 2 cm. There are two stainless steel joints at both ends of the sand pack. The upper joint is at the outlet and has a circular hole at the center of its curved surface for connecting pipes. The lower joint is at the inlet and has a side hole for connecting pipes. The structure of the sand pack is shown in Fig. 2.

2.2. Materials

The crude oil used for the experiments was extracted from an oilfield in the Bohai Sea. It was mixed with 35 wt% kerosene to obtain the required oil sample. The viscosity of the oil sample was 823.1 mPa·s at 20 °C. Deionized water was used to prepare a potassium iodide solution with a mass fraction of 5%. Potassium iodide exhibits strong X-ray absorption, increasing the water phase density and significantly enhancing the image contrast between

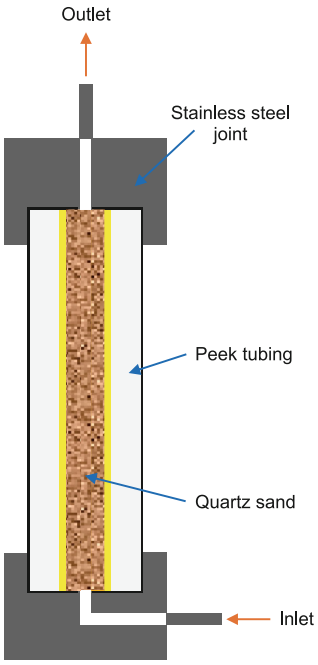

Fig. 2. Structure diagram of the sand pack.

Fig. 3. Two types of quartz sand with different particle sizes.

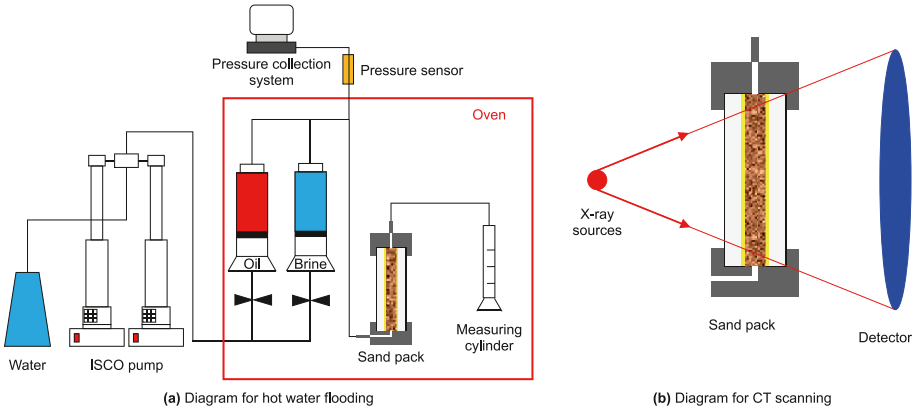

(a) Diagram for hot water flooding (b) Diagram for CT scanning

Fig. 1. Schematic of the experimental setup.

the oil, water, and rock phases. The viscosity of the water sample was 0.7 mPa·s at 20 °C. Quartz sand with particle sizes of 40–60 mesh and 100–120 mesh fill the sand pack, as shown in Fig. 3. A strongly heterogeneous sand pack model was obtained by mixing and filling the two different particle sizes of quartz sand into the sand pack.

2.3. Procedures and plans

The steps for the hot water flooding experiment in heavy oil reservoirs were as follows:

(1) In experiments (Exps.) 1–3, the mass ratios of the quartz sand with particle sizes of 40–60 mesh and 100–120 mesh were 7:3, 5:5, and 3:7, respectively. The sand was washed and dried to remove moisture and impurities. The two quartz sand types are mixed and filled to create a strongly heterogeneous sand pack model.
(2) The sand pack model was saturated with a 5 wt% potassium iodide solution at an injection rate of 1.0 mL/min. After saturating with 5 PV of the potassium iodide solution, the sand pack model was left to stand for 1 h, and the first scanning began.
(3) The sand pack model was saturated with heavy oil at an injection rate of 0.5 mL/min. After saturating with 5 PV of the oil, the sand pack model was left to stand for 1 h, and the second scanning began.
(4) The temperature of the oven was set to 80 °C. The hot water flooding began when the intermediate container and sand pack model temperatures reached 80 °C. After injecting 5 PV of the potassium iodide solution at an injection rate of 1.0 mL/min, the sand pack model was left to stand for 1 h, and the third scanning began.
(5) In experiment (Exp.) 4, quartz sand with particle sizes of 100–120 mesh was used to prepare a weakly heterogeneous model, and steps (2) to (4) were repeated.
(6) The image processing software on the workstation processed the CT scanning images. The experimental plan and parameters are shown in Table 1.

The Xradia 515 Versa CT setup operates at a 80 kV voltage and power of 7 W. It has a resolution of 1024 × 1024 and a pixel size of 3 μm. Each scanning is performed at the same location with multiple images stitched together to obtain cylindrical images with a diameter of 3 mm and a length of 20 mm. Each scanning and reconstruction takes 10 h.

2.4. Image processing

The slices obtained from CT scanning are subjected to oil-water-rock three-phase segmentation through image processing software. Data analysis is performed on the distribution of oil and water based on the segmented images.

External factors often produce noise during CT scanning, affecting the image clarity and making it difficult to accurately identify boundaries for the oil, water, and rock phases. The non-local means (NLM) filtering method improves the signal-to-noise ratio, resulting in clearer images. The basic idea behind NLM filtering is that the estimated value of the current pixel is obtained by calculating the weighted average of pixels in the image with similar neighborhood structures (Buades et al., 2005).

After filtering all CT slices, a neural network model performs oil-water-rock three-phase segmentation on the slices. Random slices are selected for manual threshold segmentation to create a training set for the neural network. The trained neural network then segments the remaining slices.

The image processing results are shown in Fig. 4. Fig. 4(a) provides the raw scanning image of the study area. Fig. 4(b) is obtained by applying NLM filtering to the raw scanned image. The oil (red), water (blue), and rock (gray) phases are segmented in Fig. 4(c) based on the grayscale values. After NLM filtering, the scanned image exhibits a significant noise reduction, significantly improving the segmentation accuracy.

The segmentation results of CT scanning the 3D images from Exp. 1 give an average porosity within the scanning area of 37.9%, while the average initial oil saturation is 85.7%. The average porosity and initial saturation values are 36.4% and 84.3%, respectively. Errors between the calculated and measured values of the average porosity and average initial saturation are below 5%, meeting the required accuracy.

3. Pore structure heterogeneity analysis

3.1. Model zoning and parameter calculation

3.1.1. Model zoning

This study proposes a statistical method for pore structure heterogeneity to investigate the influence of pore structure heterogeneity on the sand pack model and ensure reasonable analysis of the remaining oil types. The process divides 3D images from CT scanning into zones and calculates parameters for each zone. The 3D images are divided into five layers. Each layer is divided into 36 zones of the same size at 0.5 mm × 0.5 mm × 4 mm. Fig. 5(a) shows a 3D schematic of the zoning from the model, and Fig. 5(b) illustrates a two-dimensional (2D) schematic of the zoning from the CT scanning image.

3.1.2. Statistical method for average pore size

The 3D images are divided into zones after the first CT scan using the method described in Section 3.1.1. The image segmentation results allow measuring the pore volumes for each zone to calculate the total pore volume of the model. The average porosity for the model is 38.2%, consistent with the porosity obtained from the full CT scanning images, validating the feasibility of the proposed method. The formula for calculating average porosity is

Table 1
Experimental plan parameters.

Experiment	Mass of quartz sand		Average porosity, %	Average permeability, μm^2	Oil saturation, %
	40–60 mesh, g	100–120 mesh, g			
Exp. 1	0.68	0.27	36.4	6.157	84.3
Exp. 2	0.48	0.48	35.6	5.284	81.8
Exp. 3	0.27	0.67	35.3	4.725	83.1
Exp. 4	0	0.97	34.9	4.086	82.7

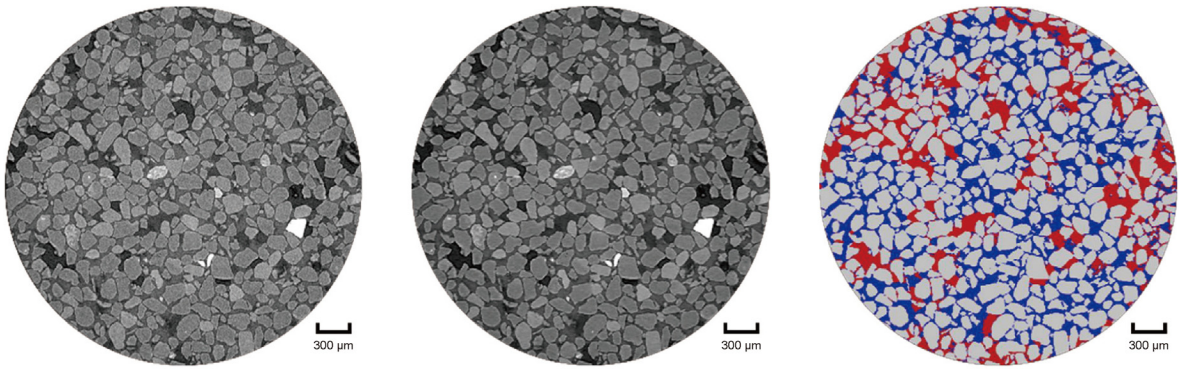

(a) Raw scanning image (b) NLM filtered image (c) Machine learning segmented image

Fig. 4. Workflow of the CT scanning image.

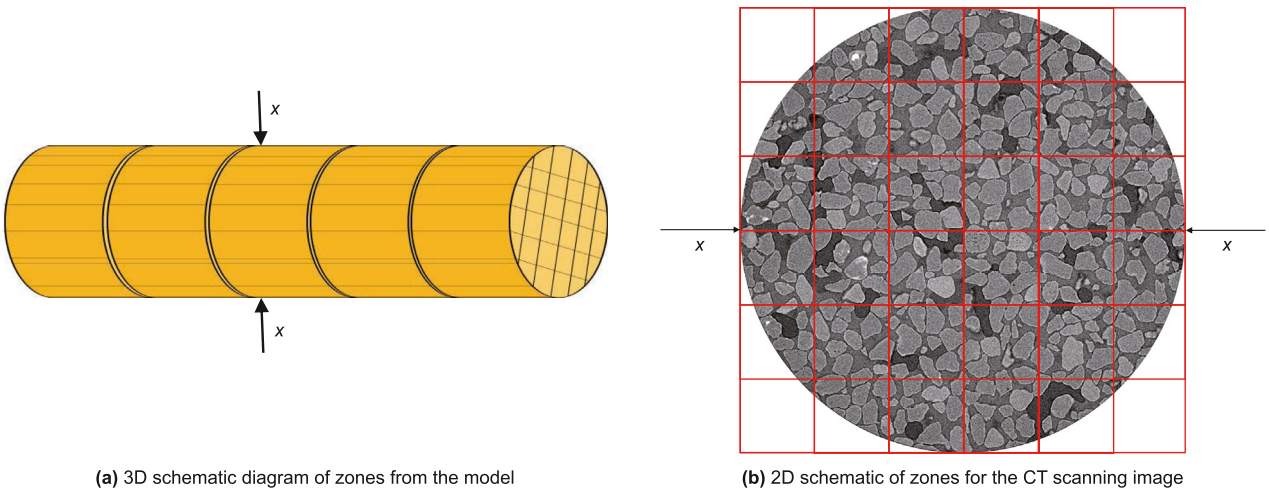

(a) 3D schematic diagram of zones from the model (b) 2D schematic of zones for the CT scanning image

Fig. 5. Schematic diagram of the zones from the model.

$$\phi_{\mathrm{cal}} = \frac{\sum_{i=1}^{n} V_{\mathrm{pore\_}i}}{V_{\mathrm{total}}} \times 100\%$$

where ϕ_{cal} is the average porosity of the model from statistical analysis of all zones, %; $V_{\mathrm{pore\_}i}$ is the pore volume within the i-th zone, μm^3; n is the number of zones; and V_{total} is the total volume of the model, μm^3.

The average pore volume of a zone is the ratio of the total pore volume within the zone to the number of pores. The formula for calculating average pore volume is

$$\overline{V}_{\mathrm{pore\_}i} = \frac{V_{\mathrm{pore\_}i}}{n_{\mathrm{pore\_}i}}$$

where $\overline{V}_{\mathrm{pore\_}i}$ is the average pore volume of the i-th zone, μm^3; and $n_{\mathrm{pore\_}i}$ is the number of pores within the i-th zone.

After obtaining the average pore volume, the average pore size is calculated based on the formula of the sphere. Thus,

$$D_{\mathrm{pore\_}i} = \left(\frac{6}{\pi} \cdot \overline{V}_{\mathrm{pore\_}i}\right)^{\frac{1}{3}}$$

where $D_{\mathrm{pore\_}i}$ is the average pore size of the i-th zone, μm.

3.1.3. Statistical method for remaining oil saturation

The 3D images are divided into zones after the third CT scanning using the method described in Section 3.1.1. The remaining oil saturation of each zone is measured based on the image segmentation results. The average remaining oil saturation of the model is calculated based on the weighted average of the pore volume in the different zones, consistent with the average remaining oil saturation of the entire model and confirming mass conservation. The formula for calculating the average remaining oil saturation is

$$S_{\mathrm{o\_cal}} = \frac{\sum_{i=1}^{n} V_{\mathrm{pore\_}i} S_{\mathrm{o\_}i}}{V_{\mathrm{pore}}} \times 100\%$$

where $S_{\mathrm{o\_cal}}$ is the average remaining oil saturation of the model obtained through zone-based statistical analysis of all zones, %; $S_{\mathrm{o\_}i}$ is the remaining oil saturation within the i-th zone, μm^3; and V_{pore} is the total pore volume of the model, μm^3.

3.2. Experimental analysis of pore structure heterogeneity

3.2.1. Analysis of 2D CT scanning images

Images of the third CT scanning of the Exps. 1 and 4 are selected to compare the average pore size and remaining oil saturation between the strongly heterogeneous and weakly heterogeneous models. The 2D CT slices after segmentation are shown in Fig. 6. In

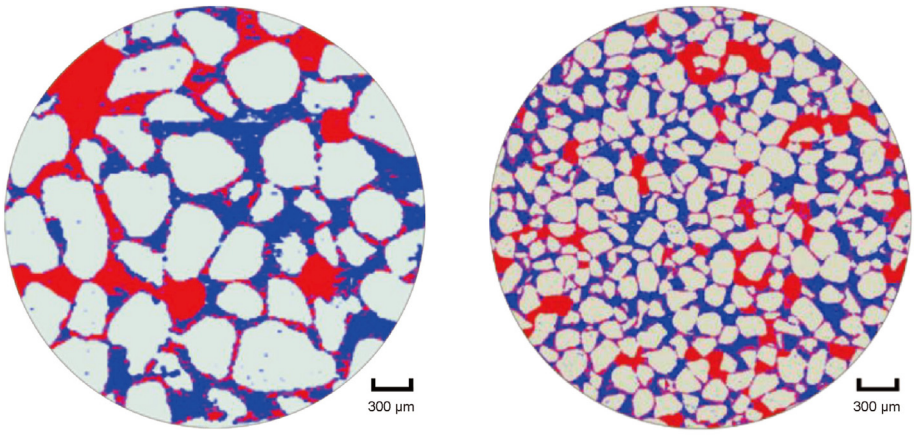

(a) Strongly heterogeneous model (Exp. 1) **(b)** Weakly heterogeneous model (Exp. 4)

Fig. 6. 2D segmented slices of the third CT scanning (red area is oil, blue area is water, and white area is rock).

the slice, the red area is the oil phase, the blue area is the water phase, and the white area is the rock. The pores are composed of a combination of red and blue area. The strongly heterogeneous model is filled with two different types of quartz sand, causing a wide distribution range for the pore size. The remaining oil distribution of the strongly heterogeneous model is continuous with a high oil saturation. The meshes of quartz sand in the weakly heterogeneous model are large and consistent, resulting in similar average pore sizes. The remaining oil distribution of the weakly heterogeneous model is disperse with a low oil saturation.

3.2.2. Description of hot water channeling channels

The average pore sizes of each zone are calculated for the models to obtain the associated distributions in the sand pack models (Fig. 7). The zones are classified into three levels: large-pore zones (average pore size over 75 μm), medium-pore zones (average pore size between 65 and 75 μm), and small-pore zones (average pore size below 65 μm). All zones are categorized following the average pore size classification.

Each zone's remaining oil saturation is calculated for each model to obtain the associated distribution in the sand pack models (Fig. 8). The oil saturation reduction in each zone during flooding is calculated based on initial and remaining oil saturations. These values allow classifying the zones into three levels: high-reduction zones (oil saturation reduction over 0.2), medium-reduction zones (oil saturation reduction between 0.1 and 0.2), and low-reduction zones (oil saturation reduction below 0.1). All zones are categorized accordingly following the oil saturation reduction classification.

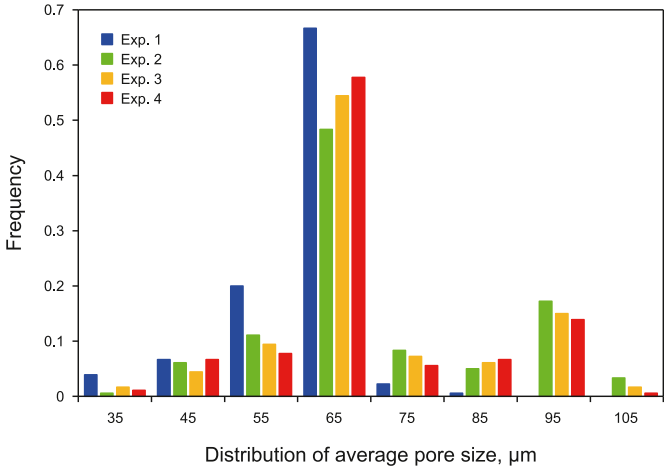

Fig. 7. Distribution of the average pore size.

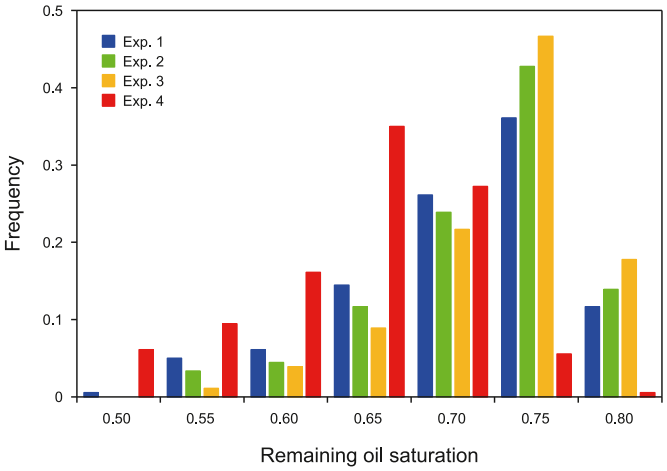

Fig. 8. Distribution of remaining oil saturation.

The size and location of the microscale channeling channels during hot water flooding are obtained based on the average pore size and remaining oil saturation within each zone. The high-reduction zones are observed as hot water channeling channels. The average pore sizes of the high-reduction zones are calculated for each layer. When a high-reduction zone is a large-pore zone, the average pore size matches the oil saturation reduction. Otherwise, they do not match. The number of matching zones compared to the total number of zones in the hot water channeling channels is defined as the matching rate, which is calculated for each layer. The formula for calculating the matching rate is

$$R_p = \frac{n_p}{n_{total}} \times 100\%$$

where R_p is the matching rate; n_p is the number of matching zones for the average pore size in one layer; and n_{total} is the number of zones in hot water channeling channels in one layer.

3.3. Classification of microscopic remaining oil

The remaining oil has various occurrence modes, and the microscopic remaining oil is usually classified based on the occurrence form and location of oil blocks. The shape factor and contact area ratio provide quantitative characterization.

The shape factor (Qin et al., 2022; Su et al., 2022; Gao et al., 2022) quantitatively characterizes the microscopic remaining oil occurrence form, defined as

$$G = \frac{6\sqrt{\pi}V}{S^{1.5}}$$

where G is the shape factor; V is the volume of an oil block, μm^3; and S is the surface area of an oil block, μm^2.

The shape factor is related to the shape complexity of an oil block. As the shape factor increases, the block becomes more regular. The shape factor also decreases in the order of droplet shape, film shape, cluster shape, and network shape.

The contact area ratio (Nie et al., 2022) quantitatively characterizes the microscopic remaining oil occurrence location, defined as

$$C = \frac{S_c}{S}$$

where C is the contact area ratio; S_c is the contact area between the oil block and the pore, μm^2; and S is the surface area of the oil block, μm^2.

The contact area ratio is used primarily to distinguish the film remaining oil from the other types. The contact area ratio of film remaining oil is close to 0.5.

It is necessary to obtain the volume, surface area, and contact area of oil blocks with the pores to calculate the shape factor and contact area ratio of an oil block. As shown in Table 2, the shape factor and contact area ratio allow dividing the microscopic remaining oil into four types: droplet, film, cluster, and network remaining oil. The 3D images for each type of microscopic remaining oil are shown in Fig. 9. The network remaining oil is a continuous phase, and the remaining three shapes are discontinuous. The shape factors of the droplet, film, cluster, and network remaining oil decrease in turn. Compared with the others, the film remaining oil is the thinnest.

4. Results and discussion

4.1. Laws of channeling channels

The remaining oil saturations in Exps. 1–4 are 73.8%, 75.3%, 75.6%, and 67.1%, respectively. The points in Fig. 10(a)–(d) show the initial and remaining oil saturations of each layer for the four experiments in turn. The remaining oil saturation gradually increases from the model inlet to the outlet. The remaining oil saturations at the inlet are 68.8%, 70.1%, 72.3%, and 63.5%, respectively, and the remaining oil saturations at the outlet are 78.6%, 79.5%, 80.2%, and 71.7%. The remaining oil saturation is greatest in Exp. 3 and lowest in Exp. 4. The strongly heterogeneous model has a greater remaining oil saturation in each layer than the weakly heterogeneous model. In Exp. 2, the strongest pore structure heterogeneity causes a high remaining oil saturation. In Exp. 3, quartz sand with small particle sizes (100–120 mesh) accounts for 70%, and few large-pore zones exist. The permeability of the model is lower than in the Exp. 2. Hot water flows along the large pores, forming narrow channeling channels. Due to the opposite effects of permeability and heterogeneity, the remaining oil saturation in Exp. 3 is nearly equal to that in Exp. 2. In Exp. 1, quartz sand with large particle sizes (40–60 mesh) accounts for 70%, and there are more large-pore zones. The permeability of the model is greater than that in Exp. 2. Due to the synergistic effects of permeability and heterogeneity, the remaining oil saturation in Exp. 1 is lower than in Exp. 2.

Table 2
Classification criteria of microscopic remaining oil.

Type of remaining oil	Shape factor G	Contact area ratio C
Droplet	$G > 0.6$	$0 < C < 1$
	$0.4 \leq G < 0.6$	$C \leq 0.45$, $C > 0.6$
Film	$0.4 \leq G < 0.6$	$0.45 < C \leq 0.6$
Cluster	$0.2 \leq G < 0.4$	$0 < C < 1$
Network	$G < 0.2$	$0 < C < 1$

After analyzing the average pore size distribution, average remaining oil saturation distribution, and the variation of oil saturation in each layer in four experiments, it is found that the models in Exps. 1–3 exhibit strong heterogeneity, and the experimental results are relatively close, with significant differences from the weakly heterogeneous model in Exp. 4. Therefore, in the subsequent analysis, Exps. 1 and 4 are selected as representatives of the strongly heterogeneous model and the weakly heterogeneous model, respectively.

Fig. 11 shows the segmented CT slices from Exps. 1 and 4. The red, blue, and white areas represent oil, water, and rock, respectively. The images are ordered from the inlet to the outlet. The oil phase content increases from the inlet to the outlet. At the same distance from the entrance, the oil content in Exp. 1 is higher than that in Exp. 4. Based on the segmented CT slices from Exps. 1 and 4, the oil saturation reductions and average pore sizes of all zones are calculated and classified in each layer of the models. The classification results are shown in Figs. 12 and 13. Based on the classification results of oil saturation reductions and average pore sizes, the matching rates of Exps. 1 and 4 are calculated and shown in Table 3.

Due to the small distribution range of the average pore size in the weakly heterogeneous model (Exp. 4) and the significant decrease in remaining oil saturation, there are fewer differences in the remaining oil saturation at various locations. Therefore, the influence of the average pore size on the oil saturation reduction is weak, and the matching rate is low. The distribution ranges for the average pore size in the strongly heterogeneous model (Exp. 1) are larger than the weakly heterogeneous model, and the oil saturation reduction is smaller because of the hot water fingering. There are significant differences in the remaining oil saturation at various locations. The average pore size significantly impacts the oil saturation reduction, and the remaining oil in large pores decreases greatly, resulting in a high matching rate.

Fig. 14 shows the oil saturation reduction levels for all zones in the strongly heterogeneous model (Exp. 1) and the weakly heterogeneous model (Exp. 4). The inlet zones show a greater oil saturation reduction in the weakly heterogeneous model, while the outlet zones show a lower reduction. There are several zones the hot water cannot reach due to fingering phenomena on the model outlet. The degree of oil saturation reduction varies greatly at different locations. The number of zones within the channeling channels accounts for 32.8% of the total number of total zones. The strongly heterogeneous model shows smaller oil saturation reduction levels in the middle and outlet zones than the weakly heterogeneous model. The outlet zones show smaller oil saturation reductions, while the significantly reduced remaining oil saturation only occurs at the inlet zones. The channeling channels in the strongly heterogeneous model are narrower than in the weakly heterogeneous model, resulting in a shorter hot water

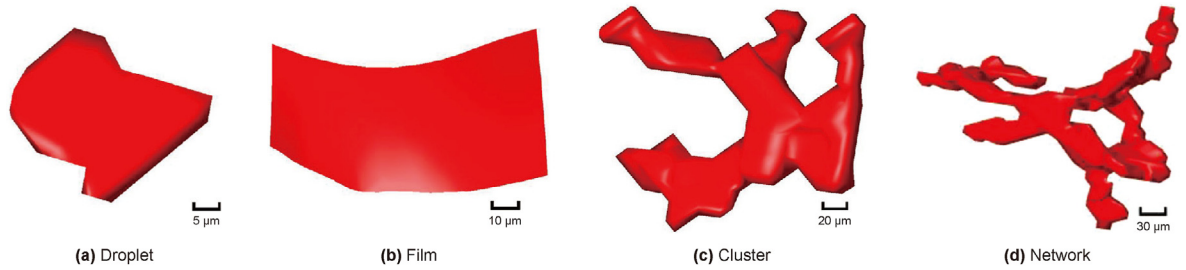

Fig. 9. 3D images of various microscopic remaining oil types.

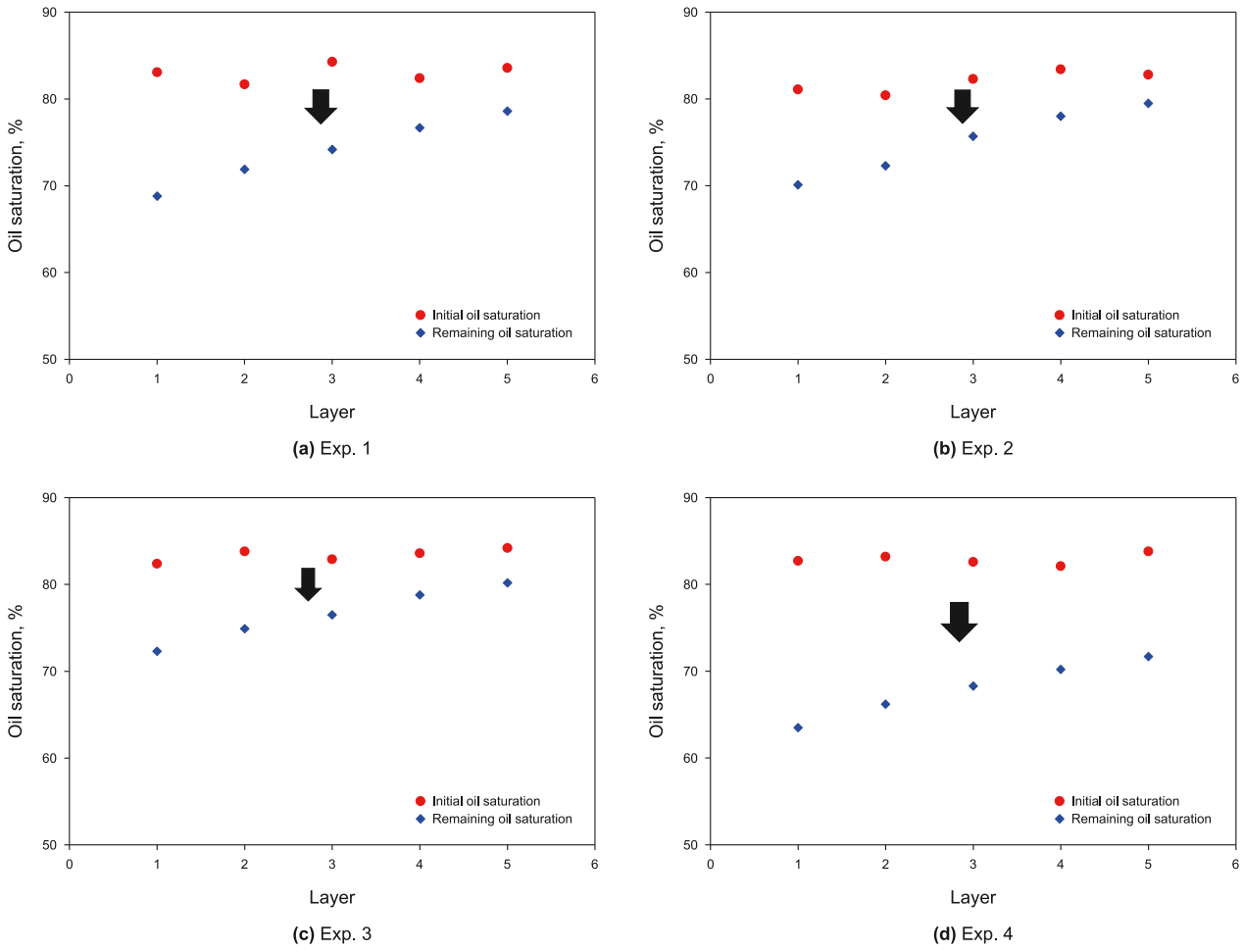

Fig. 10. Points of the oil saturation for the four considered models.

breakthrough time, more severe fingering phenomena, a lower sweep efficiency, and a lower recovery. The number of zones within the channeling channels accounts for 12.2% of the total number of total zones.

Fig. 15 is a schematic diagram of the channeling channels, where the green, red, and black areas are the channels. There is balanced hot water flooding in the weakly heterogeneous model, and oil saturation reduction in most zones is more than 20% after hot water flooding. Narrow channeling channels are formed after hot water flooding in the strongly heterogeneous models. The remaining oil saturation in other areas decreased slightly, resulting in imbalanced flooding.

4.2. Statistical laws and micro remaining oil distribution characteristics

In the strongly heterogeneous models, there are greater differences in the remaining oil between the interior and exterior of the hot water channeling channels. The study uses Exp. 1 as an example. The location of the channeling channels in the strongly heterogeneous model is described based on the levels of oil saturation reduction within the zones. The remaining oil types inside and outside the channeling channels are distinguished to obtain the volume proportions, as shown in Fig. 16. The volume proportion of network remaining oil inside the channeling channels is lower

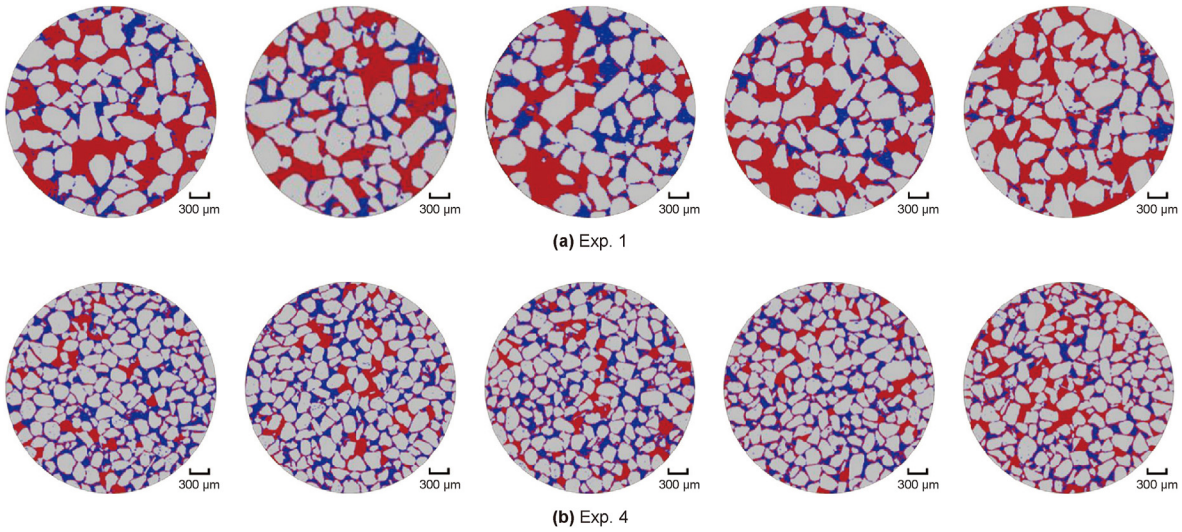

Fig. 11. 2D CT scanning slices for each layer of the models.

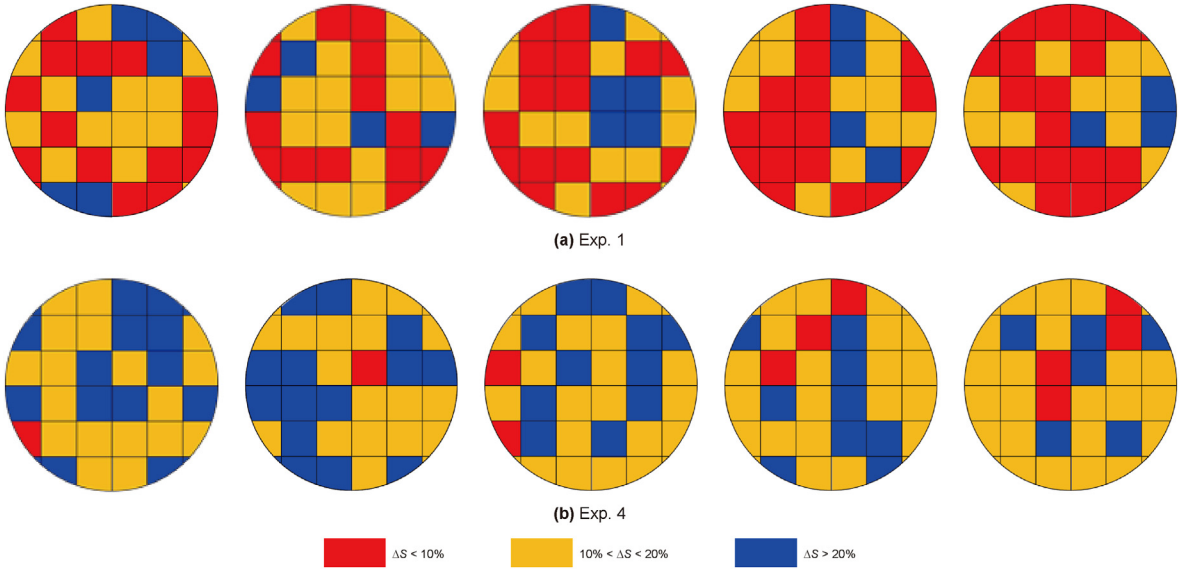

Fig. 12. Levels of oil saturation reduction for all zones (ΔS is the oil saturation reduction).

than outside, and the volume proportions of cluster, film, and droplet remaining oil are greater.

The oil phase over the entire model is continuous with a high saturation before injecting hot water. After injecting hot water, heat is transferred to the surrounding porous media and oil phase, decreasing the oil viscosity. Due to the pore structure heterogeneity of porous media, hot water tends to flow through zones with larger average pore sizes to form channeling channels. The sweep area of the hot water no longer increases once the channels form. The oil in the hot water channeling channels is displaced under the continued action of the hot water. The oil phase transforms from continuous to discontinuous, decreasing the network remaining oil volume and increasing the cluster, film, and droplet remaining oil volumes. Significant heat is lost from the hot water during the injection process. Heating the oil outside the hot water channeling channels, where the oil phase remains continuous, is difficult. The volume proportion of network remaining oil inside the channeling channels is 62.87%, and that outside the channeling channels is 81.41%. The shapes of the different remaining oil types are shown in Fig. 17.

The average network remaining oil volume and film remaining oil average thickness are shown in Table 4, which change significantly after hot water flooding. The hot water causes a portion of the network remaining oil to convert into other remaining oil types, decreasing its volume proportion. The rest of the network remaining oil is divided into multiple smaller sections, and the average volume block decreases. The hot water causes the film remaining oil on the rock surface in the channeling channels to be continuously displaced, decreasing the film remaining oil thickness on the rock surface. As the hot water cannot reach here, the oil on the rock surface is difficult to displace outside the channeling channels. Thus, the amount of film remaining oil on the rock surface is small, and the thickness is large.

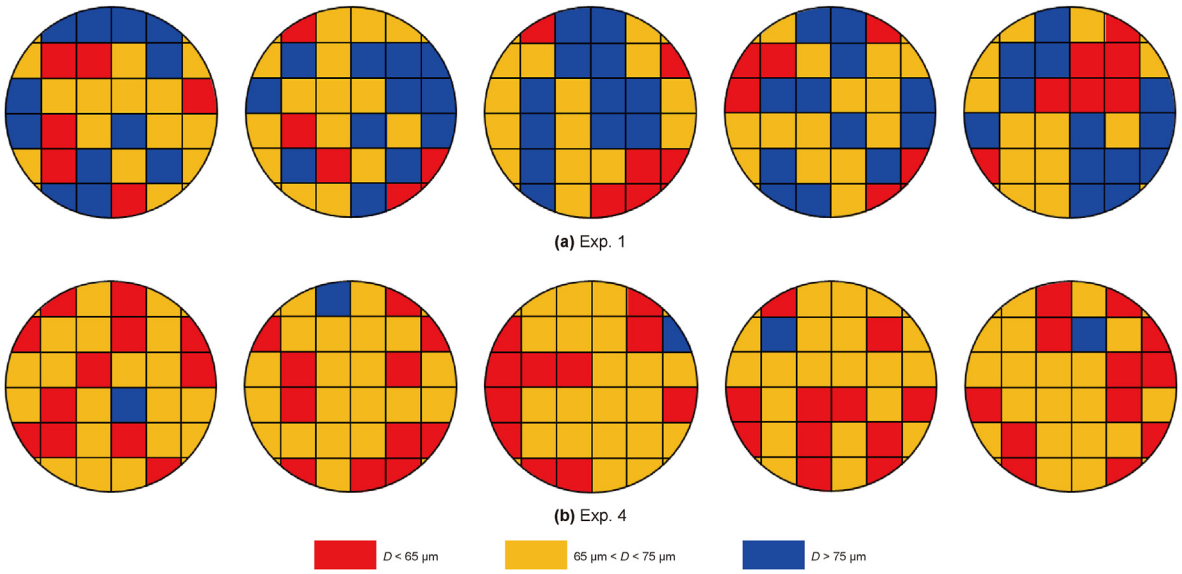

Fig. 13. Levels of average pore size for all zones (D is the average pore size).

Table 3
Matching rate in each layer.

Layer		1 (inlet)	2	3	4	5 (outlet)	Total
Matching rate, %	Exp. 1	83.3	100	100	100	100	95.5
	Exp. 4	5.9	6.7	9.1	0	16.7	8.6

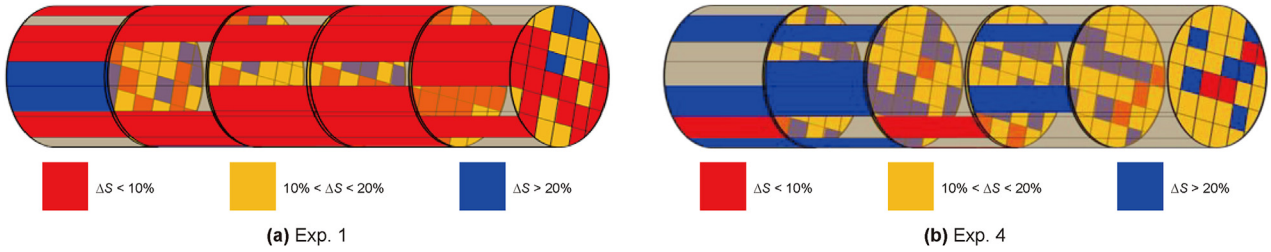

Fig. 14. Levels of oil saturation reduction.

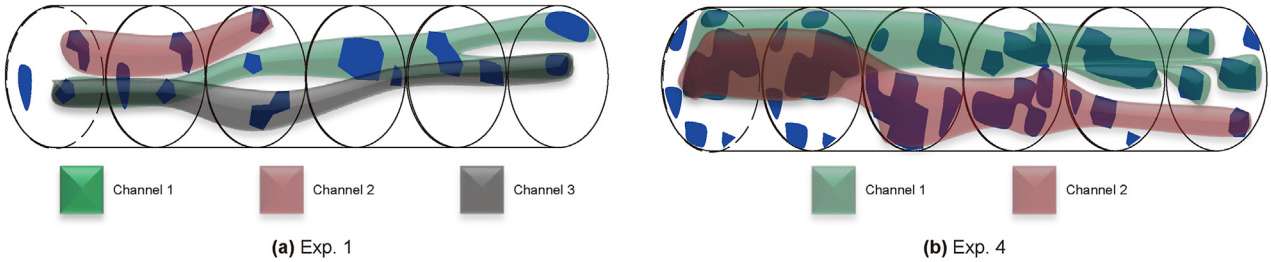

Fig. 15. Channeling channels of the models.

5. Conclusions

The influence of the pore structure heterogeneity on hot water channeling channels is studied through physical experiments. In the experiments, the strongly heterogeneous model is filled with a mixture of quartz sand of differing particle sizes to characterize the pore structure heterogeneity of the model. The 3D images of the model are obtained using CT scanning technology. A proposed zonal statistical method divides the 3D model image into 180 zones of the same size and calculates each zone's average pore sizes and oil saturation reductions. A method is proposed to determine the average pore size and oil saturation reduction levels. The zones where the oil saturation reduction is above 20% are considered hot water channeling channels. The matching rate is proposed to characterize the relationship between the average pore size and oil saturation reduction. Finally, the shape factor and contact area ratio

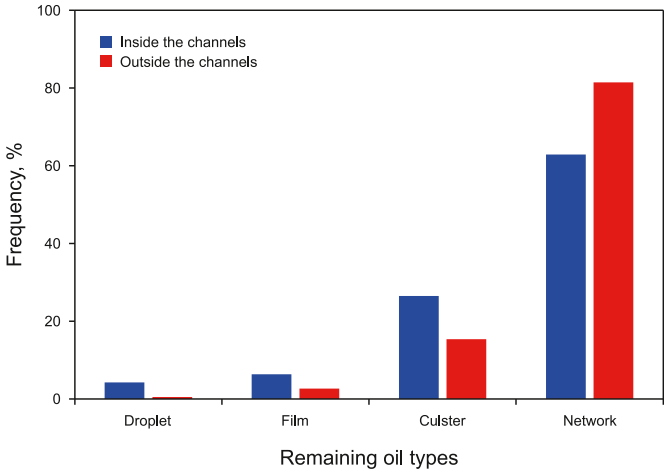

Fig. 16. The volume proportions for various remaining oil types.

are used to evaluate heavy oil to divide the microscopic remaining oil into four types: network, cluster, film, and droplet. The volume proportions of different remaining oil types inside and outside the channeling channels are analyzed, and the following conclusions are drawn.

(1) Hot water flooding experiments were conducted for the weakly heterogeneous models (Exp. 4) and strongly heterogeneous models (Exps. 1–3). The initial oil saturations of the models in Exps. 1–4 were 84.3%, 81.8%, 83.1%, and 82.7%, respectively. At the final stage of hot water flooding, the remaining oil saturations of the models in Exps. 1–4 were 73.8%, 75.3%, 75.6%, and 67.1%.

(2) The average pore sizes and oil saturation reductions for all zones in the weakly heterogeneous and strongly heterogeneous models were calculated. In the weakly heterogeneous model (Exp. 4), the influence of the average pore size on the oil saturation reduction is insignificant, and the total matching rate of all zones is only 8.6%. In the strongly heterogeneous model (Exp. 1), the average pore size significantly impacts the oil saturation reduction, and the remaining oil in large pores decreases greatly, and the total matching rate of all zones is nearly 100%.

(3) The 3D distribution of hot water channeling channels is shown based on the oil saturation reduction levels for all zones. Hot water flooding is balanced in the weakly heterogeneous model (Exp. 4), and the channeling channel zones account for 32.8% of the total zones. Severe fingering phenomena lead to imbalanced hot water flooding in the strongly heterogeneous model (Exp. 1), and the zones of channeling channels only account for 12.2% of the total zones. In the weakly heterogeneous model, zones with larger average pore sizes have greater oil saturation reductions. In the strongly heterogeneous model, the average pore size for most zones within the channeling channels is greater than the maximum average pore size of the weakly heterogeneous model.

(4) In the strongly heterogeneous model (Exp. 1), the volume proportion of the network remaining oil inside the channeling channels is lower than outside the flow channeling channels. The hot water flooding transforms the network

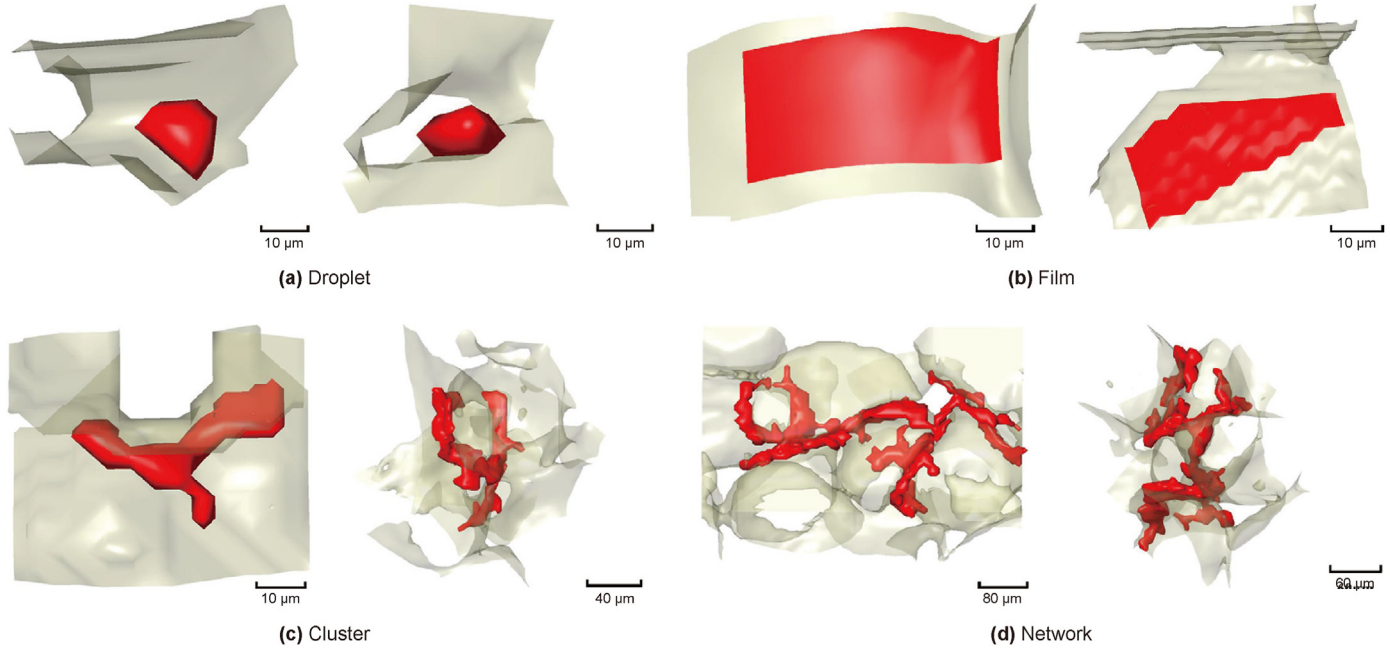

Fig. 17. The shapes of different types of remaining oil (red area is oil and gray area is rock).

Table 4
Parameters of the remaining oil.

Parameter	Inside channeling channels	Outside channeling channels
Average network remaining oil bock volume, μm^3	4826.7	8146.2
Average film remaining oil block thickness, μm	6.9	16.3

remaining oil into several cluster, film, and droplet remaining oil. The volume proportion of network remaining oil inside the channeling channels is 62.9%, and that outside is 81.4%. The average volume of the network remaining oil blocks and average thickness of the film remaining oil blocks decrease significantly during hot water flooding.

CRediT authorship contribution statement

Qing-Jun Du: Writing – review & editing, Conceptualization. **Hao-Yu Zheng:** Writing – original draft, Methodology. **Jian Hou:** Resources, Funding acquisition. **Yong-Ge Liu:** Software, Formal analysis. **Jian-Fang Sun:** Project administration, Investigation. **Dong Zhao:** Data curation.

Declaration of competing interest

The authors declare that they have no known competing financial interests or personal relationships that could have appeared to influence the work reported in this paper.

Acknowledgments

This work was supported by the National Key Research and Development Program of China (Grant No. 2018YFA0702400), the National Natural Science Foundation of China (Grant No. 52174050), the Natural Science Foundation of Shandong Province (Grant No. ZR2020ME088), and the National Natural Science Foundation of Qingdao (Grant No. 23-2-1-227-zyyd-jch).

References

Ado, M.R., Greaves, M., Rigby, S.P., 2019. Numerical simulation of the impact of geological heterogeneity on performance and safety of THAI heavy oil production process. J. Petrol. Sci. Eng. 173, 1130–1148. https://doi.org/10.1016/j.petrol.2018.10.087.

Buades, A., Coll, B., Morel, J.-M., 2005. A non-local algorithm for image denoising. In: IEEE Computer Society Conference on Computer Vision and Pattern Recognition (CVPR'05), vol. 2, pp. 60–65. https://doi.org/10.1109/CVPR.2005.38.

Chen, Q., Liu, Y., Hou, J., et al., 2023. Phase transition characteristics of heavy oil-viscosity reducer-water emulsion systems. J. Mol. Liq. 379, 121638. https://doi.org/10.1016/j.molliq.2023.121638.

Cheng, B., Li, J., Jiang, S., et al., 2021. Pore-scale investigation of microscopic remaining oil variation characteristic in different flow rates using micro-CT. Energies 14 (11), 3057. https://doi.org/10.3390/en14113057.

Ding, B., Dong, M., Chen, Z., Kantzas, A., 2022a. Enhanced oil recovery by emulsion injection in heterogeneous heavy oil reservoirs: experiments, modeling and reservoir simulation. J. Petrol. Sci. Eng. 209, 109882. https://doi.org/10.1016/j.petrol.2021.109882.

Ding, L., Jouenne, S., Gharbi, O., et al., 2022b. An experimental investigation of the foam enhanced oil recovery process for a dual porosity and heterogeneous carbonate reservoir under strongly oil-wet condition. Fuel 313, 122684. https://doi.org/10.1016/j.fuel.2021.122684.

Dong, X., Jiang, X., Zheng, W., et al., 2022. Discussion on the sweep efficiency of hybrid steam-chemical process in heavy oil reservoirs: an experimental study. Petrol. Sci. 19 (6), 2905–2921. https://doi.org/10.1016/j.petsci.2022.06.018.

Dong, X., Liu, H., Chen, Z., et al., 2019. Enhanced oil recovery techniques for heavy oil and oilsands reservoirs after steam injection. Appl. Energy 239, 1190–1211. https://doi.org/10.1016/j.apenergy.2019.01.244.

Fang, Y., Yang, E., Guo, S., Cui, C., Zhou, C., 2022. Study on micro remaining oil distribution of polymer flooding in Class-II B oil layer of Daqing Oilfield. Energy 254, 124479. https://doi.org/10.1016/j.energy.2022.124479.

Gao, Y., Xie, X., Wang, S., et al., 2022. Pore-scale experimental investigation of the remaining oil formation in water-wet, mixed-wet and oil-wet sandstone samples. J. Petrol. Sci. Eng. 216, 110790. https://doi.org/10.1016/j.petrol.2022.110790.

Gu, X., Pu, C., Khan, N., et al., 2019. The visual and quantitative study of remaining oil micro-occurrence caused by spontaneous imbibition in extra-low permeability sandstone using computed tomography. Fuel 237, 152–162. https://doi.org/10.1016/j.fuel.2018.09.014.

Guo, C., Wang, X., Wang, H., et al., 2018. Effect of pore structure on displacement efficiency and oil-cluster morphology by using micro computed tomography (μCT) technique. Fuel 230, 430–439. https://doi.org/10.1016/j.fuel.2018.05.058.

Hou, J., Li, Z., Zhang, S., et al., 2009. Computerized tomography study of the microscopic flow mechanism of polymer flooding. Transport Porous Media 79 (3), 407–418. https://doi.org/10.1007/s11242-008-9330-9.

Hu, B., Chai, G., Liu, X., et al., 2023. Insights into the microscopic oil-water flow characteristics and displacement mechanisms during waterflooding in sandstone reservoir rock based on micro-CT technology: a pore-scale numerical simulation study. Materials 16 (9), 3555. https://doi.org/10.3390/ma16093555.

Jiang, N., Zhang, Z., Qu, G., et al., 2022. Distribution characteristics of micro remaining oil of Class III reservoirs after fracture flooding in Daqing Oilfield. Energies 15 (9), 3385. https://doi.org/10.3390/en15093385.

Jing, W., Zhang, L., Li, A., et al., 2022. Investigation of pore-scale remaining oil dynamic evolution in heterogeneous marine carbonate using real-time computed tomography scanning. Energy Fuels 36 (15), 8180–8188. https://doi.org/10.1021/acs.energyfuels.2c01497.

Leng, J., Wei, M., Bai, B., 2022. Impact of polymer rheology on gel treatment performance of horizontal wells with severe channeling. SPE J. 27 (2), 1017–1035. https://doi.org/10.2118/209190-PA.

Li, J., Liu, Y., Gao, Y., et al., 2018a. Effects of microscopic pore structure heterogeneity on the distribution and morphology of remaining oil. Petrol. Explor. Dev. 45 (6), 1112–1122. https://doi.org/10.1016/S1876-3804(18)30114-9.

Li, L., Zhou, X., Su, Y., et al., 2022. Influence of heterogeneity and fracture conductivity on supercritical CO_2 miscible flooding enhancing oil recovery and gas channeling in tight oil reservoirs. Energy Fuels 36 (15), 8199–8209. https://doi.org/10.1021/acs.energyfuels.2c01587.

Li, Y., Jia, H., Pu, W., et al., 2023. Investigation of feasibility of alkali-cosolvent flooding in heavy oil reservoirs. Petrol. Sci. 20 (3), 1608–1619. https://doi.org/10.1016/j.petsci.2022.12.001.

Li, Z., Sun, X., Wang, F., et al., 2018b. Microscopic flow characteristics of fluids in porous medium and its relationship with remaining oil distribution: a case study in Saertu oil field of Daqing in China. Geofluids 2018, 7549831. https://doi.org/10.1155/2018/7549831.

Lin, Z., Lu, X., Imran, M.Knorr, Zeng, F., 2023. Experimental study of viscous fingering in sand-pack model for heavy oil reservoir. Chem. Eng. Res. Des. 191, 271–285. https://doi.org/10.1016/j.cherd.2023.01.022.

Liu, H., Dong, X., 2022. Current status and future trends of hybrid thermal EOR processes in heavy oil reservoirs. Petrol. Sci. Bull. 7 (2), 174–184 (in Chinese).

Liu, Y., Dong, X., Chen, Z., et al., 2021. Pore-scale movability evaluation for tight oil enhanced oil recovery methods based on miniature core test and digital core construction. Ind. Eng. Chem. Res. 60 (6), 2625–2633. https://doi.org/10.1021/acs.iecr.0c04256.

Liu, Y., Hu, W., Cao, J., et al., 2018. Diagenetic constraints on the heterogeneity of tight sandstone reservoirs: a case study on the Upper Triassic Xujiahe Formation in the Sichuan Basin, southwest China. Mar. Petrol. Geol. 92, 650–669. https://doi.org/10.1016/j.marpetgeo.2017.11.027.

Liu, Y., Zhang, C., Li, S., Li, Z., 2023. Study of steam heat transfer enhanced by CO_2 and chemical agents: in heavy oil production. Petrol. Sci. 20 (2), 1030–1043. https://doi.org/10.1016/j.petsci.2022.09.034.

Masoomi, R., Torabi, F., 2022. A new computational approach to predict hot-water flooding (HWF) performance in unconsolidated heavy oil reservoirs. Fuel 312, 122861. https://doi.org/10.1016/j.fuel.2021.122861.

Nie, C., Wu, X., Hou, Z., Li, J., Jiang, H., 2022. Evaluation of the factors influencing residual oil evolution after alkali/surfactant/polymer flooding in Daqing Oilfield. Energies 15 (3), 1048. https://doi.org/10.3390/en15031048.

Qin, X., Xia, Y., Wu, J., et al., 2022. Influence of pore morphology on permeability through digital rock modeling: new insights from the Euler number and shape factor. Energy Fuels 36 (14), 7519–7530. https://doi.org/10.1021/acs.energyfuels.2c01359.

Rezaeiakmal, F., Parsaei, R., Shafiabadi, A., Rezaei, A., 2022. Insights into the flow behaviour of the pre-generated polymer enhanced foam in heterogeneous porous media during tertiary oil recovery: effect of gravitational forces. J. Petrol. Sci. Eng. 213, 110385. https://doi.org/10.1016/j.petrol.2022.110385.

Spooner, V.E., Geiger, S., Arnold, D., 2021. Dual-porosity flow diagnostics for spontaneous imbibition in naturally fractured reservoirs. Water Resour. Res. 57 (5), e2020. https://doi.org/10.1029/2020WR027775. WR027775.

Su, Y., Zha, M., Jiang, L., et al., 2022. Pore structure and fluid distribution of tight sandstone by the combined use of SEM, MICP and X-ray micro-CT. J. Petrol. Sci. Eng. 208, 109241. https://doi.org/10.1016/j.petrol.2021.109241.

Sun, P., Xu, H., Zhu, H., et al., 2021. Investigation of pore-type heterogeneity and its control on microscopic remaining oil distribution in deeply buried marine clastic reservoirs. Mar. Petrol. Geol. 123, 104750. https://doi.org/10.1016/j.marpetgeo.2020.104750.

Sun, X., Song, Z., Cai, L., et al., 2020. Phase behavior of heavy oil-solvent mixture systems under reservoir conditions. Petrol. Sci. 17, 1683–1698. https://doi.org/10.1007/s12182-020-00461-x.

Wang, D., Liu, F., Li, G., et al., 2023. Characterization and dynamic adjustment of the flow field during the late stage of waterflooding in strongly heterogeneous reservoirs. Energies 16 (2), 831. https://doi.org/10.3390/en16020831.

Wang, M., Li, L., Zhou, Y., et al., 2022. Experimental study on the effect of microheterogeneity on multiphase flow in a microscopic visualization model. Energy Fuels 36 (9), 4757–4769. https://doi.org/10.1021/acs.energyfuels.2c00146.

Wang, Y., Liu, H., Zhang, Q., et al., 2020. Pore-scale experimental study on EOR mechanisms of combining thermal and chemical flooding in heavy oil reservoirs. J. Petrol. Sci. Eng. 185, 106649. https://doi.org/10.1016/j.petrol.2019.106649.

Wang, Y., Liu, H., Zhou, Y., 2021. Development of a deep learning-based model for the entire production process of steam-assisted gravity drainage (SAGD). Fuel 287, 119565. https://doi.org/10.1016/j.fuel.2020.119565.

Wei, P., Pu, W., Sun, L., et al., 2018. Oil recovery enhancement in low permeable and severe heterogeneous oil reservoirs via gas and foam flooding. J. Petrol. Sci. Eng. 163, 340–348. https://doi.org/10.1016/j.petrol.2018.01.011.

Xu, F., Chen, Q., Ma, M., et al., 2020. Displacement mechanism of polymeric surfactant in chemical cold flooding for heavy oil based on microscopic visualization experiments. Adv. Geo Energy Res. 4 (1), 77–85. https://doi.org/10.26804/ager.2020.01.07.

Yang, J., Shan, G., Wang, Z., et al., 2023. Experimental study of distribution and quantitative characterization of discontinuous oil phase based on micro-CT. Front. Earth Sci. 11, 1117971. https://doi.org/10.3389/feart.2023.1117971.

Yang, Y., Tao, L., Iglauer, S., et al., 2020. Quantitative statistical evaluation of micro residual oil after polymer flooding based on X-ray micro computed-tomography scanning. Energy Fuels 34 (9), 10762–10772. https://doi.org/10.1021/acs.energyfuels.0c01801.

Zhang, Z., Jin, Y., Zhang, J., et al., 2022. Adaptability study of hot water chemical flooding in offshore heavy oilfields. Geofluids 2022, 1–11. https://doi.org/10.1155/2022/2224321.

Zhao, D.W., Gates, I.D., 2015. On hot water flooding strategies for thin heavy oil reservoirs. Fuel 153, 559–568. https://doi.org/10.1016/j.fuel.2015.03.024.

Zhao, W., Zhao, L., Jia, P., Wang, P., Hou, J., 2022. Influence of micro-heterogeneity of fractured-porous reservoirs on the water flooding mobilization law. Energy Technol. 53, 102694. https://doi.org/10.1016/j.seta.2022.102694.